Editors' Suggestion | Featured in Physics

Hydrodynamic Elastocapillary Morphing of Hair Bundles

Jonghyun Ha,[1] Yun Seong Kim,[1] Kaiying Jiang,[1] Ryan Siu,[1] and Sameh Tawfick[1,2,*]
[1]Department of Mechanical Science and Engineering, University of Illinois at Urbana-Champaign, Urbana, Illinois 61801, USA
[2]The Beckman Institute for Advanced Science and Technology, University of Illinois at Urbana-Champaign, Urbana, Illinois 61801, USA

(Received 18 March 2020; revised 30 June 2020; accepted 11 November 2020; published 16 December 2020; corrected 13 January 2021)

We report polymorphic self-assembly of hair arranged in hollow bundles driven by capillarity, hydrodynamics, and elasticity. Bundles emerging from a liquid bath shrink but remain hollow at slow drainage due to the negative pressure of the menisci trapped between the hairs. The timescale allows the collective stiffening of the fibers to resist closure. At fast drainage, the bundles fully close before the liquid can drain through the hair. A liquid column trapped in the hole closes the bundle while the lubricated hairs still behave softly. Scaling laws predict this reversible hair polymorphism.

DOI: 10.1103/PhysRevLett.125.254503

Very long aspect ratio hairs in liquid exhibit intriguing synchronized motion and self-assembly. For instance, the functionality of biological cilia is enabled by their synchronized beating, large elastic deformation, and constant rearrangement [1]. At the nanoscale, carbon nanotubes self-assemble into curious patterns during drying [2,3]. These unusual patterns are observed when large numbers of dense hairs rearrange due to capillarity. These beautiful phenomena have induced scientists to study elastocapillarity, where capillary pressure readily deforms soft slender materials [4–6], and liquid rise in soft solids [7,8]. Recently, interesting new phenomena were observed when self-assembly of soft hair is driven at higher rates, leading to polymorphic self-assembly related to hydrodynamics [9–11]. The rich solid-liquid phenomena at the transition from static capillarity to hydrodynamics are unexplored, and, more importantly, the understanding of the timescale of the transition from slow aggregation to synchronous beatinglike motion is absent.

Here, we study the self-assembly of wet hair that exhibits rate-dependent self-assembly [9,10] to understand the transition from static capillarity to hydrodynamic polymorphism. Hairlike carbon fibers are assembled perpendicular to a base having a ring-shaped cross section, forming a hollow bundle that we refer to as a "hairy-wall tube," which differs from a regular hair bundle by having an inner hole [Fig. 1(a) and Movie S1 in Supplemental Material [12]]. Hair is immersed in a liquid container, and, depending on the bundle's diameter, height, and the drain rates as they pierce the liquid-to-air interface, we observe two distinct deformation modes of the hollow bundles. Bundle shrinkage without hole closure is observed for short bundles and slow rates, while a single radial beat leading to complete closure occurs for long bundles and at fast rates. We had previously observed capillary-induced twisting of hairs for softer bundles having a smaller number of hairs and at high speeds [10]. In the current study, we investigate a larger range of drain rates and bundle geometries to explore the various deformation modes as a function of hair length,

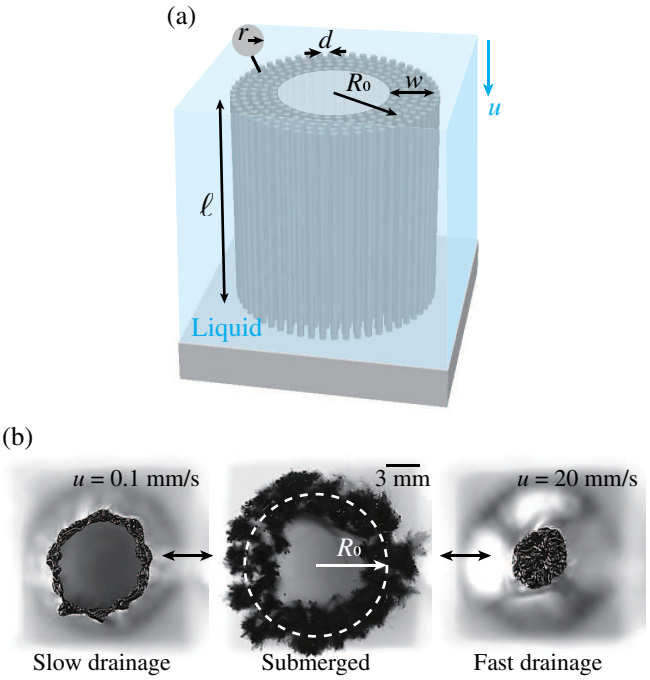

FIG. 1. Hydrodynamic elastocapillarity-induced polymorphism of hairy tubes. (a) Schematics of hairy tubes. R_0, w, r, d, and ℓ correspond to the inner radius, the thickness of the tubes, fiber radius, spacing, and length, respectively. (b) Top views of the hairy tubes ($R_0 = 7$ mm, $\ell = 25$ mm). The middle image indicates the shape of the initial state. The left and right images indicate the final shape of the partial closure (slow drainage, $u = 0.1$ mm/s) and the complete closure (fast drainage, $u = 20$ mm/s), respectively.

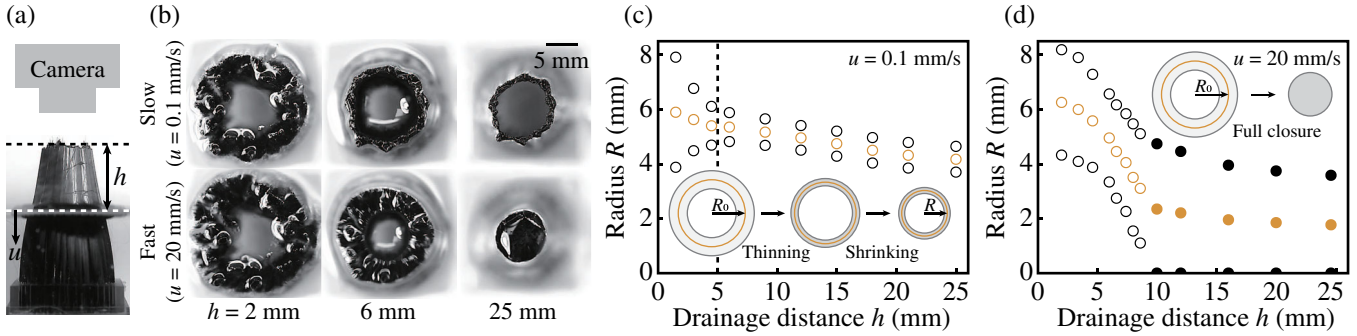

FIG. 2. Evolution of tube closure. (a) Side view of hairy tubes ($R_0 = 7$ mm, $\ell = 25$ mm). The ring-shaped images are captured by a top camera. (b) Drainage distance evaluation of tube closure. Top and bottom images correspond to slow ($u = 0.1$ mm/s) and fast drainage ($u = 20$ mm/s), respectively. h and R correspond to the drainage distance and the contracted radius, respectively. Movie S1 [12] shows the reversibility between partial and complete closure. (c) Fiber densification and shrinking regimes of partial closure at slow drainage. The left side from the dashed line indicates fiber densification, and the right side indicates shrinking (partial closure). (d) Diameter evolution during complete closure at fast drainage. Empty and filled symbols correspond to the partial and complete closure, respectively. Orange circle markers correspond to the average radius between outer and inner radii. Upper and lower black circle markers correspond to the outer and inner radius, respectively.

organization, liquid properties, and drain dynamics (see S1 in Ref. [12]). The coupling between capillarity, hydrodynamics, and elasticity leading to polymorphism has implications on other areas of physics and materials.

We fabricate the hairy tube by inserting carbon fiber bundles into a circular hole pattern on a base (see S2 in Ref. [12]). Then, we submerge the hairy tubes and then push the base out of the water using a motorized linear stage (EAS series, Orientalmotor), as shown in Fig. 1(a). The drainage velocity u is defined as the set speed of the linear stage. The middle image in Fig. 1(b) shows the top view of the immersed hairy tubes with length ℓ and hole radius R_0. Once the tubes pierce the water interface, fibers assemble due to surface tension. The pattern selection is set by ℓ, R_0, and u. The same hair bundle morphs from one geometry to another as a function of u. For short bundles and especially in the slow-drainage regime (low u), the holes shrink but resist full closure: The hair organization remains as hollow tubes with dense hairs at the wall, as shown in the left image in Fig. 1(b). We refer to this shrinkage as partial closure. However, the holes completely close at fast drainage (high u), as shown in the right image in Fig. 1(b). Therefore, the interaction of bundle geometry (elastocapillarity) and drainage hydrodynamics determines the morphology of assembled hairs.

To explain this morphing phenomenon, we get insights by tracking the kinematics of hole closure to plot the mean radius of the bundle, R, as we increase the drainage distance h, during the lowering of the water interface. Figure 2(a) shows the experimental setup. The evolution of R is quite different between the two cases, i.e., slow and fast drainage. During slow drain, the hairs locally coalesce first, and the tube wall thins before the mean diameter starts shrinking as shown in the top images in Fig. 2(b). Initially, the outer radius of the tube contracts while the inner radius increases [see Fig. 2(c)]. In the later stage, both outer and inner radii of the tubes shrink. Interestingly, in the fast-drainage conditions, the order of the two stages flips: We observe hole closure where the fibers move inward in a synchronized fashion before wall thinning. The hairs also appear fully submerged during the initial hole closure at fast drain rate as shown in the bottom images in Fig. 2(b) and the plot in Fig. 2(d).

We schematically plot our understanding of the slow-drainage mechanism in Fig. 3(a). This assembly is governed by balance between capillary forces in the small menisci between fibers and the collective stiffening of the dense fibers. The densification and fiber rearrangement are critical to take into consideration to understand the resistance of the bundle to full closure in the slow regime. By considering the surface energy of annular bundles, we show that the tangential (hoop) force F_c can be written as $F_c \sim \gamma h$, where γ is the surface tension (see S3 in Ref. [12] and also Ref. [13]). This force also results from the long meniscus trapped between dense fibers in circular arrangement, and the relation captures the intuitive increase in F_c with the increase in the meniscus height h as the liquid is drained [Fig. 3(a)]. We note that the contact angle between the fibers and the liquid is 20°. The elastic resistance results not only from the simple bending of individual hairs, but also from the contact resistance and hair rearrangement during slow drainage. We consider a fibrous array where the fibers sequentially contact each other, and their resistance increases as they densify. In this dense case, the elastic force is $F_e \propto \delta^2$, where δ is the hair deflection as they come in contact during the radial shrinkage of the hollow bundle (see S3 in Ref. [12]). In particular, as δ increases, the thickness of the tube walls will increase, leading to packing into a dense arch. The packing of the fibers effectively leads to higher resistance to capillary compression. By taking account of the reorganization of hair in the hollow bundle and the packing effects, we can get the final form of the elastic tangential

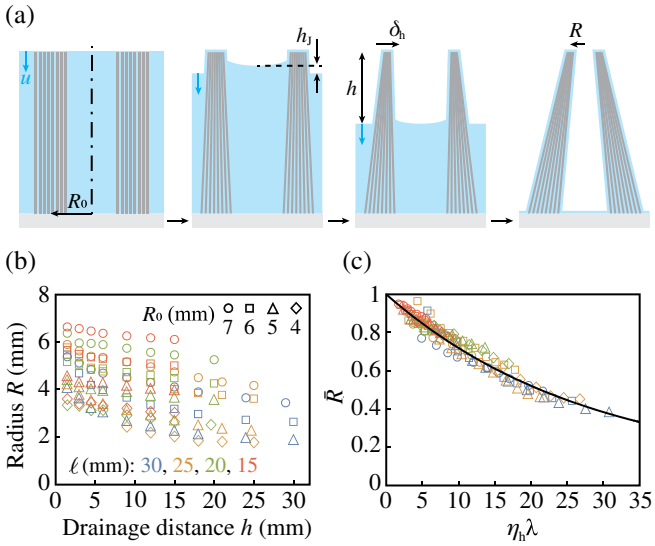

FIG. 3. Capillarity-driven partial closure at slow drainage. (a) Schematics of a side view of slow-drainage mechanism. The drainage process goes from left to right. (b) Experimentally measured tube radii versus drainage distance for various bundle geometries. (c) Nondimensional $\bar{R}$ versus drainage distance $\eta_h\lambda$, where λ is the aspect ratio. The experimental data collapse onto a single line when plotted against our scaling law, Eq. (1).

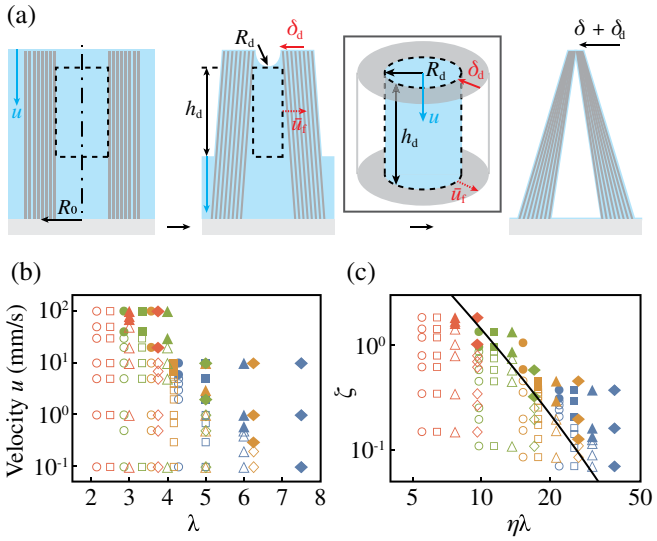

FIG. 4. Hydrodynamic-driven full closure at fast drainage. (a) Schematics of a side view of fast-drainage mechanism. The black box corresponds to the control volume of mass conservation. The drainage process goes from left to right. (b) Regime map of hair morphing where λ is the aspect ratio. Empty and filled symbols correspond to the partial and complete closure, respectively. (c) Universal regime map where ζ is the dimensionless dynamic rise and $\eta\lambda$ is the dimensionless drainage height with respect to ℓ_{ec}. The black line corresponds to the transition from partial to complete closure according to the theoretical model, Eq. (3). According to the theoretical line, the lower and upper regions indicate partial and complete closure, respectively. The markers for different geometries are listed in Fig. 3(b).

$F_e \sim \alpha EIR_0\delta^2/[r\ell^3(R_0-\delta)]$, where E and I are the Young's modulus and second moment of area of a single fiber, respectively (see S3 in Ref. [12]). The structural coefficient α can be written as $\alpha = \alpha_p w\rho_0/(r\rho_f)$, where ρ_0 and ρ_f are the fiber area fraction of the top surface in the initial and final shape, respectively (see S3 in Ref. [12]). α_p is a prefactor. Please note that F_e is dependent on stiffening and rearrangement, and, without this added complexity, the model would incorrectly predict full closure at any drain rate. We parametrize $\delta_h = \delta(h)$ to analyze the kinematics of the slow drainage as a function of the quasistatic drain height.

The force balance $F_c \sim F_e$ leads to $\gamma h \sim \alpha EIR_0\delta_h^2/[r\ell^3(R_0-\delta_h)]$. Noting the relation between the circumferential and radial deflections, we define $\bar{\delta}_h = \delta_h/R_0$ as the dimensionless radial deflection, $\eta_h = (h\ell)^{1/2}/\ell_{ec}$ as a kinematic elastocapillary number, and $\lambda = \ell/R_0$ as the aspect ratio of the hollow tubes. The length $\ell_{ec} = [EI/(r\gamma)]^{1/2}$ is the elastocapillary length balancing the surface tension and the stiffness of a fiber [4]. The dimensionless force balance reads $(\eta_h\lambda)^2 \sim \alpha\bar{\delta}_h{}^2/(1-\bar{\delta}_h)$, showing the scaling between the elastocapillarity of the hollow bundle (left) and the shrinkage (right). By solving a quadratic equation of $\bar{\delta}_h$, we obtain

$$\bar{\delta}_h \sim \frac{[(\eta_h\lambda)^4 + 4\alpha(\eta_h\lambda)^2]^{1/2} - (\eta_h\lambda)^2}{2\alpha}, \qquad (1)$$

describing the shrinkage not only as a function of the length, but also the instantaneous drainage height through the use of η_h. To corroborate the kinematic model, we normalize the measured $R(=R_0-\delta_h)$ by R_0, which leads to the nondimensional contracted radius $\bar{R} = 1-\bar{\delta}_h$ in Fig. 3(b) according to our scaling law [Eq. (1)] in Fig. 3(c). We observe that the experimental data for various tube geometries (see S1 in Ref. [12]) are collapsed onto a single master curve despite the various number of fibers, consistent with our theory. This result highlights that, for slow drain rates, the self-assembly is governed by static elastocapillarity, where fiber densification and stiffening due to rearrangement play a critical role in determining the final morphology.

The hollow bundle fully collapses (hole closure) at fast drainage, as shown in Fig. 4 and Movie S1 [12]. Figure 4(b) shows the hole closure regime map by experimentally varying the drain speed and geometry of the bundles. Qualitatively, during fast drainage, a long liquid column, $h_d \gg h_J$ [see Figs. 3(a) and 4(a)], is trapped in the bundle during the drainage and causes the full closure. This column is governed by viscous dissipation, which takes place at the fiber spacing d. The liquid drainage through the fiber spacings is restricted due to large viscous stresses within the narrow d, trapping a tall column in the bundle hole. The negative capillary pressure within this dynamic rise pulls the soft wall, causing it to completely close.

The competition between the timescales of fiber aggregation (bundle wall thinning) τ_a and inner diameter closure (flopping) τ sets the transition between slow and fast drainage (see S4 in Ref. [12]). At slow drainage, where the viscous dissipation can be neglected, fiber aggregation precedes inner diameter closure $\tau_a < \tau$ versus $\tau < \tau_a$ at a fast drain rate.

A scaling law governs the formation of a tall liquid column within the inner hole of the tube, leading to complete closure, as schematically shown in Fig. 4(a). Calculating h_d as a function of drain velocity u can be used for the scaling of the dynamic capillary force f_c. The bundles behave very softly, so the radius of the liquid meniscus on the top of the tube, R_d, is formed obeying Jurin's law $h_d \sim \gamma/(\rho g R_d)$, where ρ and g are liquid density and the gravitational acceleration, respectively [14]. Along h_d, R_d generates negative pressure (see S5 in Ref. [12]). The timescale is set when the negative pressure pulls the bundle wall inward, generating a relative liquid flow in the outward direction. Considering viscous resistance ($\sim \mu \bar{u}_f w$) and compression ($\sim \Delta p d^2$) at a single pore, we can express the relative velocity $\bar{u}_f \sim (d^2/\mu)\Delta p/w$, where d is the length scale of the fluid conduit (fiber spacing). The pressure difference Δp is induced by capillarity and can be scaled as γ/R_d. Thus, $\bar{u}_f \sim (d^2/\mu)(\gamma/R_d)/w$. Applying mass conservation between vertical and radial flow, the relative radial flow rate can be expressed as $Q_f \sim \bar{u}_f h_d R_d$, and the flow rate of the liquid column in the vertical direction is $Q_h \sim u R_d^2$, when it reaches the steady state. Considering the continuity of the flows in vertical and radial directions, $Q_f = Q_h$, we get $h_d \sim u R_d/\bar{u}_f$. By using the relation $\bar{u}_f$ and $R_d \sim \gamma/(\rho g h_d)$, we finally express $h_d \sim [\gamma \mu w u/(\rho g d)^2]^{1/3}$.

Using h_d, we write the dynamic capillary force as $f_c \sim \Delta p A_d$. The capillary pressure within the column, $\Delta p \sim \gamma/R_d$, leads to the complete closure of the hollow bundle at fast drainage. The surface area of the liquid column in the tube scales as $A_d \sim R_d h_d$. Thus, the dynamical compression force can be written as $f_c \sim \gamma h_d$. Because the hairs do not have time to densify, they behave as a soft noninteracting structure before the tube wall thinning, as opposed to their collective stiffening in the slow-drainage rate. We can express $f_e \sim \beta R_0 E I \delta_d/(r\ell^3)$, where δ_d is the dynamical deflection and $\beta = \beta_p w \rho_0/r$ is a structural coefficient of noncoalesced fibers (see S6 in Ref. [12]). β_p is a prefactor. Normalizing the force balance, $f_c \sim f_e$, leads to $\gamma h_d \sim \beta R_0 E I \delta_d/(r\ell^3)$ and divided by R_0 provides

$$\bar{\delta}_d \sim (\eta\lambda)^2 \zeta \beta^{-1}, \tag{2}$$

where $\bar{\delta}_d = \delta_d/R_0$ is dimensionless deflection due to dynamic effects and $\eta = \ell/\ell_{\mathrm{ec}}$ is the elastocapillary number. We note that η_h becomes η when h reaches ℓ. Parameter $\zeta = h_d/\ell$, governed by u, is the dimensionless dynamical rise height. We found that both the static and dynamic compression forces play a role in bundle closure. When the water base is below the fiber base (h reaches ℓ), the tubes undergo further deformation $\bar{\delta}$, related to capillary-induced fiber aggregation. We express $\bar{\delta}$ by replacing η_h in Eq. (1) with η. The nondimensional contracted radius of the final shape can be written as $\bar{R} = 1 - (\bar{\delta} + \bar{\delta}_d)$. When $\bar{R} = 0$, the tubes completely close, as shown in Fig. 4(a). Combining the relation $\bar{\delta}$ and Eq. (2), we can provide the scaling law of the complete closure:

$$\zeta \sim \frac{\beta}{(\eta\lambda)^2}(1 - \bar{\delta}), \tag{3}$$

where $\bar{\delta}$ is computed from Eq. (1) by replacing h with ℓ. The scaling law of Eq. (3) involves the dynamic rise effects (ζ), capillary-driven deformation effects (η), and the bundle geometry (λ). This is used to transform the regime map in Fig. 4(b) into the universal scaling law in Fig. 4(c). The hairy tubes completely close at high λ and u, which correspond to long ℓ (large flexibility) and small R_0. Even when the magnitude of the total deflection is small, it is enough to collapse the tubes with relatively small R_0. The drain dynamics set the collective stiffness of the bundle, making it behave softly or stiffly at fast and slow u, respectively. The equation $\bar{R} = 1 - \Omega$, where $\Omega = \bar{\delta} + \bar{\delta}_d$, is the dimensionless total deflection. The black curve in Fig. 4(c) is obtained when $\bar{\delta} + \bar{\delta}_d = 1$ and marks the transition between partial and complete closure (see S7 in Ref. [12]). In the region of $\zeta > 1$, where u is very fast, and small $\eta\lambda$, the scaling law has minor disagreements with the experiments. On the other hand, we confirm that these laws predict the behavior of, for instance, liquids with much higher viscosity (see S8 in Ref. [12]).

We have presented an experimental system to study fluid-structure interactions of dense flexible structures, exhibiting clear transition from static-capillarity-driven to hydrodynamic-driven assembly. This leads to polymorphism from open (annular) to closed bundles based on the drain rate. The phenomenon also manifests itself in other complex patterns such as triangular and multihole bundles (see S9 and Movie S2 in Ref. [12]). In particular, we find that the hairs collectively stiffen at slow drain rates to shrink without collapse, but, at faster rates, the liquid is trapped within the hole in the bundle and within the wall, leading to a soft behavior and full closure. We developed universal scaling laws to predict the kinematics of hole shrinkage during slow drainage and the transition from partial or complete closure, and these laws work for various liquid viscosities. We anticipate the current work to pave the way for developing reconfigurable shape-shifting systems which are actuated via capillarity, such as artificial muscles [15], soft robotics, and smart textiles.

This work was supported by AFOSR Young Investigator Program (Grant No. FA9550-19-1-0010), NSF CMMI (Grant No. 1825758), and National Research Foundation of Korea (Grant No. 2019R1A6A3A03032230).

*tawfick@illinois.edu

[1] A. Vilfan and F. Jülicher, Hydrodynamic Flow Patterns and Synchronization of Beating Cilia, Phys. Rev. Lett. **96**, 058102 (2006).
[2] S. Tawfick, J. Bico, and S. Barcelo, Three-dimensional lithography by elasto-capillary engineering of filamentary materials, MRS Bull. **41**, 108 (2016).
[3] M. Volder, S. Tawfick, S. J. Park, D. Copic, Z. Zhao, W. Lu, and A. Hart, Diverse 3D microarchitectures made by capillary forming of carbon nanotubes, Adv. Mater. **22**, 4384 (2010).
[4] A. Cohen and L. Mahadevan, Kinks, rings, and rackets in filamentous structures, Proc. Natl. Acad. Sci. U.S.A. **100**, 12141 (2003).
[5] J. Bico, B. Roman, L. Moulin, and A, Boudaoud, Elastocapillary coalescence in wet hair, Nature (London) **432**, 690 (2004).
[6] H.-Y. Kim and L. Mahadevan, Capillary rise between elastic sheets, J. Fluid Mech. **548**, 141 (2006).
[7] C. Duprat, J. Aristoff, and H. A. Stone, Dynamics of elastocapillary rise, J. Fluid Mech. **679**, 641 (2011).
[8] J. Ha and H.-Y. Kim, Capillarity in soft porous solids, Annu. Rev. Fluid Mech. **52**, 263 (2020).
[9] D. Shin and S. Tawfick, Polymorphic elastocapillarity: Kinetically reconfigurable self-assembly of hair bundles by varying the drain rate, Langmuir **34**, 6231 (2018).
[10] L. Kovanko and S. Tawfick, Capillary-induced hair twist, Langmuir **35**, 13421 (2019).
[11] A. Hadjittofis, J. R. Lister, K. Singh, and D. Vella, Evaporation effects in elastocapillary aggregation, J. Fluid Mech. **792**, 168 (2016).
[12] See Supplemental Material at http://link.aps.org/supplemental/10.1103/PhysRevLett.125.254503 for includes details of samples preparations, theoretical derivations, and "additional experimental results."
[13] J. Bico and D. Quéré, Rise of liquids and bubbles in angular capillary tubes, J. Colloid Interface Sci. **247**, 162 (2002).
[14] J. Jurin, An account of some experiments shown before the Royal Society; with an enquiry into the cause of the ascent and suspension of water in capillary tubes, Phil. Trans. R. Soc. London **30**, 739 (1718).
[15] P. Chen, Y. Xu, S. He, X. Sun, S. Pan, J. Deng, D. Chen, and H. Peng, Hierarchically arranged helical fibre actuators driven by solvents and vapours, Nat. Nanotechnol. **10**, 1077 (2015).

Correction: The name of the second author in Ref. [13] was processed improperly during the prepublication stage and has been fixed.